Int J Clin Exp Med 2018;11(7):6607-6617
www.ijcem.com /ISSN:1940-5901/IJCEM0078193

Original Article

Effect of dihydroartemisinin on invasion, migration, and apoptosis of neuroma cells by regulating the CX3CR1 signaling pathway

Yan Wang[1*], Zhenkun Zong[2*], Weiqiang Li[3], Di Wu[3], Xia Liu[3]

[1]Department of Neurosurgery, No. 6 People's Hospital of Xuzhou City, Xuzhou City, Jiangsu Province, P.R. China; [2]Department of Neurosurgery, The Affiliated Hospital of Xuzhou Medical University, Xuzhou City, Jiangsu Province, P.R. China; [3]Department of Pathology, Xuzhou Central Hospital, Xuzhou City, Jiangsu Province, P.R. China. [*]Equal contributors and co-first authors.

Received April 19, 2018; Accepted May 11, 2018; Epub July 15, 2018; Published July 30, 2018

Abstract: Objective: To elucidate mechanisms by which dihydroartemisinin (DHA) induces the apoptosis of neuroma cells by regulating the CX3CR1 signaling pathway. Methods: The U251 cell line was cultured *in vitro* and randomly assigned to the following 6 groups after transfection and treatment: the Blank group (controls), the DHA (50 μmol/L) group (with low-concentration DHA), the DHA (75 μmol/L) group (with moderate-concentration DHA), the DHA (100 μmol/L) group (with high-concentration DHA), the si-CX3CR1 group, and the DHA (100 μmol/L) + si-CX3CR1 group. qRT-PCR and Western blot analysis were conducted to detect the mRNA and protein levels of CX3CR1, the upstream ligand CX3CL1, and the downstream AKT. The apoptotic signals Caspase-3, Bcl-2, and FADD, were also detected along with activated p-AKT. The CCK-8 assay was conducted to determine changes in cell proliferation. Wound healing and transwell assays were performed to detect migration and invasion profiles of transfected cells. Flow cytometry analysis was done to examine the apoptosis profile. Results: As compared to the Blank group, the mRNA and protein expression of CX3CL1, CX3CR1, Bcl-2, and AKT declined. Whereas p-AKT expression declined, mRNA and protein expression of Caspase-3 and FADD rose substantially in the DHA (50 μmol/L) group, the DHA (75 μmol/L) group, the DHA (100 μmol/L) group, and the si-CX3CR1 group (all $P<0.05$). With the rise of DHA concentrations, the mRNA and protein expression of CX3CL1, CX3CR1, Bcl-2 and AKT were decreased more significantly, while Caspase-3 mRNA and protein expression were increased more remarkably. When compared to the Blank group, proliferation, invasion and migration of cells at different time points were attenuated in the DHA (50 μmol/L) group, the DHA (75 μmol/L) group, the DHA (100 μmol/L) group, and the si-CX3CR1 group, but the apoptosis rates became higher (all $P<0.05$). With the increase in DHA concentration, proliferation, invasion, and migration of cells at distinct time points were inhibited, and apoptosis rates were increased sequentially (all $P<0.05$). The apoptotic rates of cells in the Blank group, the DHA (50 μmol/L) group, the DHA (75 μmol/L) group, the DHA (100 μmol/L) group, the si-CX3CR1 group, and the DHA (100 μmol/L) + si-CX3CR1 group were (13.14±1.23)%, (32.95±3.26)%, (48.52±4.21)%, (62.35±6.12)%, (65.57±7.52)% and (64.52±6.85)%, respectively. Conclusion: DHA can inhibit invasion and migration of neuroma cells by inhibiting the CX3CR1 signaling pathway, thereby promoting apoptosis of neuroma cells.

Keywords: Dihydroartemisinin, CX3CR1 signaling pathway, neuroma cell, proliferation, apoptosis, migration, invasion

Introduction

Neuroma refers to schwannoma originated from the nerve sheath tissue. A majority of neuromas are located in the armpits, clavicle, limbs, neck, and other parts of the body and grow slowly. Clinically, radio-chemotherapy and surgery are currently the primary modalities of treating neuroma, but the efficacy is unsatisfactory. With the development of life science, gene therapy, and targeted therapy have become dominant modalities for the treatment of cancer. Dihydroartemisinin (DHA), a derivative of artemisinin, was initially used in the management of various subtypes of malaria, and is associated with rapid control of its clinical seizures and symptoms [1]. Additionally, DHA has also been shown to exert an inhibitory effect on

tumors, enhance the sensitivity and tolerance of tumor cells to chemotherapy drugs and radiotherapy, and improve the therapeutic effect [2]. Additionally, DHA has an inhibitory effect on cancer development (pancreatic, lung, and prostate) [3]. It improves the efficacy of temozolomide in glioma cells by inducing autophagy [4]. It also exerts anti-tumor activity by inducing apoptosis of mitochondria and endoplasmic reticulum in glioblastoma cells and death of autophagic cells [5]. Fractalkine ligand CX3CL1 is a transmembrane protein and chemokine implicated in leukocyte adhesion and migration. CX3CR1-encoded protein is a fractalkine receptor/ligand [6, 7]. Silencing of CX3CR1 can promote proliferation, migration, invasion, and apoptosis of Huh7, a hepatocellular carcinoma cell line [8]. The purpose of this study was to elucidate the effect of DHA at different concentrations on glioma U251 cells, and explore the underlying mechanisms by which DHA induces invasion, migration, and apoptosis of neuroma cells by regulating CX3CR1 signaling pathway.

Materials and methods

Materials

U251, a human glioma cell line, was bought from the cell bank of the Chinese Academy of Sciences, then resuscitated and cultured in DMEM medium (Gibco, USA) containing 10% fetal bovine serum (Gibco, USA) in a humid incubator (Thermo, USA) at 37°C in 5% CO_2. Once the density of the cells reached 90%, the cells were digested with 0.25% trypsin and subcultured at a ratio of 1:3.

Cell randomization

U251 cells in exponential phase were selected. The cell suspensions were seeded in 6-well plates at 5 * 10^4 per well, and then incubated in fresh complete medium until the cells reached 50-80% confluence, followed by transfection and associated assays. The cells were subdivided into the Blank group, the DHA (50 μmol/L) group (with low-concentration DHA), the DHA (75 μmol/L) group (with moderate-concentration DHA), the DHA (100 μmol/L) group (with high-concentration DHA), the si-CX3CR1 group, and the DHA (100 μmol/L) + si-CX3CR1 group. The cells in the Blank group were untreated. Those in the DHA low-concentration group, the DHA moderate-concentration group, and the DHA high-concentration group were cultured after addition of DHA at different concentrations (50, 75, and 100 μmol/L, respectively). The cells in the si-CX3CR1 group were treated with CX3CR1 knockdown by means of liposomal transfection. After CX3CR1 knockdown, the cells in the DHA high-concentration + si-CX3CR1 group were cultured by adding 100 μmol/L of DHA. The transfection sequence comprised forward, 5'-ACCATTGGCCTGGTGGGAAATTTT-3' and reverse, 5'-AT-TTCCCACCAGGCCAATGGTTTT-3'. The liposomal transfection was performed following the instructions on the Lipofectamine 2,000 kits (11668-027, Invitrogen, USA). The liposomes were transferred to serum-free medium Opti-MEM (Gibco, Cal, USA) for culture. Cell transfection was performed according to the instructions on the lipofectamine 2,000 kits (Invitrogen, Car, Cal, USA). Lipo solution included 240 ul of serum-free medium plus 10 ul of lipo (250 ul in total) was incubated for 5 minutes. Plasmid solution included 20 ul of serum-free medium plus 4 ug of plasmids (24 ul in total). The lipo and the plasmid solution were mixed and cultured at room temperature for 20 minutes. The mixture was added dropwise to the wells, followed by plate shaking and gentle mixing of the solution. The cells were incubated at 37°C in 5% CO_2 for 24 hours. After the 24 hour incubation, fresh medium was replaced. Forty-eight hours later, the green fluorescent protein (GFP) expression was observed under a microscope and the transfection efficiency of the cells was tested.

qRT-PCR

Total RNA was extracted from cells by means of TRIzol RNA reagents (Invitrogen, Cal, USA). Reverse transcription was conducted with the use of the Primescript TMRTreagent Kit (RRO37A, TaKaRa, Dalian, China). A fluorescence quantitative PCR instrument (ABI 7500, Applied Biosystems, USA) was used for amplification of the target genes and the reference genes. qRT-PCR was performed under the following cycling conditions: initial 40 cycles of denaturation at 94°C for 5 min, denaturation at 94°C for 30 s, denaturation at 58°C for 45 s, denaturation at 72°C for 30 s, followed by extension at 72°C for 10 min. All the reactions were performed in triplicate on different plates in the same well position. qRT-PCR was normalized to GAPDH. mRNA expression of CX3CL1,

Table 1. PCR primer sequences

	Sequence
CX3CL1	Forward: 5'-CGCGCAATCATCTTGGAGAC-3'
	Reverse: 5'-CATCGCGTCCTTGACCCAT-3'
CX3CR1	Forward: 5'-ACTTTGAGTACGATGATTTGGCT-3'
	Reverse: 5'-GGTAAATGTCGGTGACACTCTT-3'
Caspase-1	Forward: 5'-TTTGTTTGTGTGCTTCTGAGCC-3'
	Reverse: 5'-ATTCTGTTGCCACCTTTCGG-3'
Bcl-2	Forward: 5'-CTGGTGGGAGCTTGCATCAC-3'
	Reverse: 5'-CTCTCAAAGATGCCCAGGAG-3'
FADD	Forward: 5'-GCTGGCTCGTCAGCTCAAA-3'
	Reverse: 5'-ACTGTTGCGTTCTCCTTCTCT-3'
AKT	Forward: 5'-CTACCCACACAGCAGTACGC-3'
	Reverse: 5'-AAGTCGCTGGTGTTAAGCCG-3'
GAPDH PMID: 11846609	Forward: 5'-CGTCTTCACCACCATGGAGA-3'
	Reverse: 5'-CGGCCATCACGCCACAGTTT-3'

CX3CR1, Caspase-1, Bcl-2, FADD, and AKT was calculated by the $2^{-\Delta\Delta CT}$ method (PMID: 11846609). Primer sequences are shown in **Table 1**.

Western blot

Cells were lysed for extracting total protein (lysate, C0481, Sigma, USA) and bicinchoninic acid protein assay (BCA) was used for quantitative analysis. Twenty μg of sample was loaded in each well mixed with 10% SDS-PAGE gel and heated to 100°C for 5 minutes and then cool on ice. The sample was centrifuged and moved to lanes by pipettes for electrophoretic separation, followed by placing the separated protein onto the nitrocellulose membrane prepared in advance. After blocking with 5% non-fat powdered milk for 1 hour, CX3CL1 rabbit anti-human antibody (ab25088, Abcam, USA; 1:1500), CX3CR1 rabbit anti-human antibody (ab8021cam, USA; 1:1000), Caspase-1 rabbit anti-human antibody (ab1872, Abcam, USA; 1:2000), Bcl-2 rabbit anti-human antibody (ab59348, Abcam, USA; 1:15,000), FADD rabbit anti-human antibody (ab108601, Abcam, USA; 1:1,500), AKT rabbit anti-human antibody (ab8805, Abcam, USA; 1:1000) and p-AKT rabbit anti-human antibody (Ser473, SAB, USA) were added, followed by incubation at 4°C overnight. The membrane was washed with TBST three times the next day for 5 minutes per wash. HRP-conjugated goat anti-rabbit IgG (Beijing ComWin Biotech, Beijing, China; 1:500) was added and then incubated the membrane at room temperature for 1.5 hours before washing the membrane with TBST. Chemiluminescence reagents (NCI4106, Pierce, USA) were used for quantitative observation of protein expression. GAPDH was used as an internal reference gene. Mouse anti-beta-actin (1:500; Beijing ComWin Biotech, Beijing, China) was used as a primary antibody and HRP marked goat anti-mouse IgG (1:2000; Beijing ComWin Biotech, Beijing, China) was added and incubated as above. Gray values were analyzed with Image J (Bio-rad) software according to the relative expression of ECX3CL1, CX3CR1, Caspase-1, Bcl-2, and FADD calculated from the ratio of optical density of ECX3CL1, CX3CR1, Caspase-1, Bcl-2, and FADD to that of β-actin band. The procedure was repeated three times.

Cell proliferation by CCK-8 assay

The grouped cells were plated into 96-well plates. Cell culture medium (100 μL) was added to each well, and the cell density was adjusted to $2 * 10^3$/ml per well. The plates were placed in a cell incubator and incubated at 37°C, and cell viability was determined at 24 h, 48 h and 72 h, respectively. After addition of 10 μL CCK8 Reagent (C0037, Beyotiem Biotechnology, Shanghai, China) to each well, the cells were incubated at 37°C. Absorbance was examined with a microplate reader (Multiskan FC, Thermo, New York, USA), and the optical density (OD) values ranged from 450 nm to 630 nm. Three parallel wells were set in each group to acquire the mean OD value. Each test was performed in triplicate. Cell viability curves were plotted with time point as the x axis and the OD values as the y axis. Every assay was carried out in triplicate.

Cell migration by wound healing assay

Six sets of 6-well plates were selected and the corresponding cells were grouped. Horizontal lines transversely crossing the wells were evenly marked with a marker pen at spaces of 0.5 to 1 cm in the back of each 6-well plate, with at least 5 lines crossing each well. Cells were

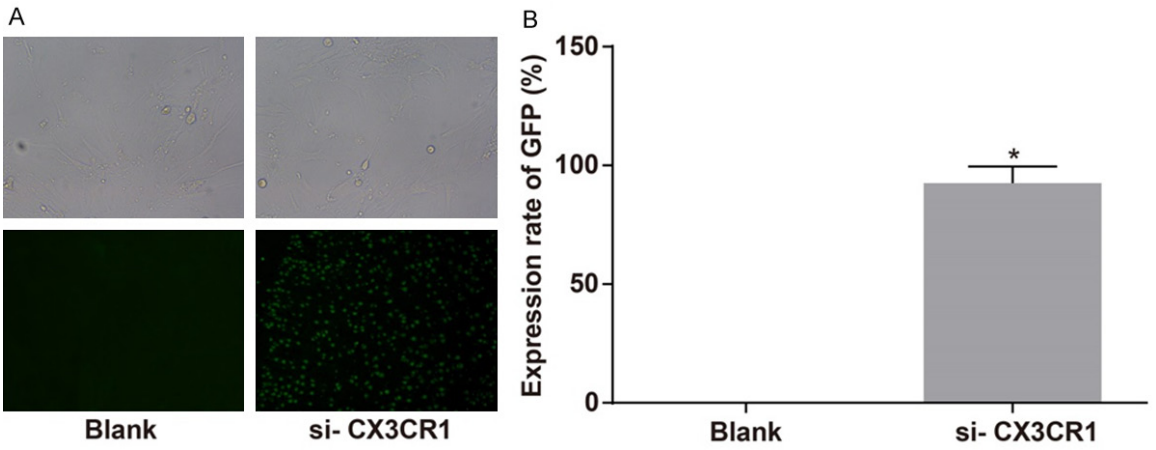

Figure 1. Verification of transfection efficiency. Note: A: GFP expression was observed under a fluorescence microscope (200×); B: Expression rate of GFP; *P<0.05, compared with the Blank group.

seeded in 6-well plates at 5 * 10^5 per well and cultured overnight. The following day, a wound was created with a pipet tip perpendicular to each horizontal line. The cells were washed with PBS three times to remove scratched cells. After addition of serum-free medium, the cells were cultured in an incubator at 37°C in 5% CO_2. The cells were sampled and photographed at 0, 12, and 24 hours, respectively. Images were acquired under an inverted microscopy at 40× magnification; the scratch-wound distance was measured. Each test was done in triplicate.

Cell invasion by the transwell invasion assay

Mataigel matrix at 50 mg/L (Sigma, SF, USA) was diluted at 1:8. Diluent (60 μL) was added to the upper surface of membranes at the bottom of each transwell chamber, and air-dried at room temperature. Unnecessary liquid in the culture plate was pipetted. Serum-free medium (50 μL) containing 10 g/L BSA was added to each well and kept standing for 30 minutes at room temperature. The cells in logarithmic phase were extracted from each group. The density of the cells was adjusted to 1 * 10^5/mL using serum-free medium containing 10 g/L BSA, and 200 μL of cell suspension was added into each chamber. Subsequently, 500 μL of cultures containing 100 mL/L FBS was added into the lower chamber of a 24-well plate. After that, the transwell chamber was transferred to a culture plate and cultured in an incubator at 37°C in 5% CO_2. After 24 hours of consecutive culture, the transwell chamber was removed, and excessive cells on the PVPF membranes were wiped off by cotton sticks. The chamber was fixed with 95% alcohol for 30 minutes, stained with Giemsa for 20 min, and washed 3 times with clean water. Cell count and image acquisition were performed under an inverted microscopy (CKX41SF inverted optical microscope, OLYMPUS, Japan). Each experiment was performed in triplicate.

Cell apoptosis by flow cytometry

Forty-eight hours after randomization, the cells were digested with trypsin without EDTA. After digestion, the cells were harvested, placed in a flow tube, and centrifuged to remove the supernatant. The cells were then rinsed three times with cold PBS, and centrifuged to remove the supernatant. Annexin-V-FITC, PI, and HEPES buffer solutions were prepared at a ratio of 1:2:50 into Annexin-V-FITC/PI staining solution following the instructions on the Annexin-V-FITC Cell Apoptosis Assay kits (C1065, Beyotime Biotech, Shanghai, China). In 100 μL of staining solution, 1 * 10^6 cells were re-suspended, and mixed by shaking. After incubation at room temperature for 15 minutes, 1 mL of HEPES buffer solution was added, and mixed by shaking. The excitation wavelength was recorded with 488 nm on the flow cytometry, and the bandpass filters corresponding to the wavelength of 525-620 nm were employed to detect FITC and PI fluorescence intensity, and the proptosis of cells, respectively. There were three samples in each group, and each test was made in triplicate.

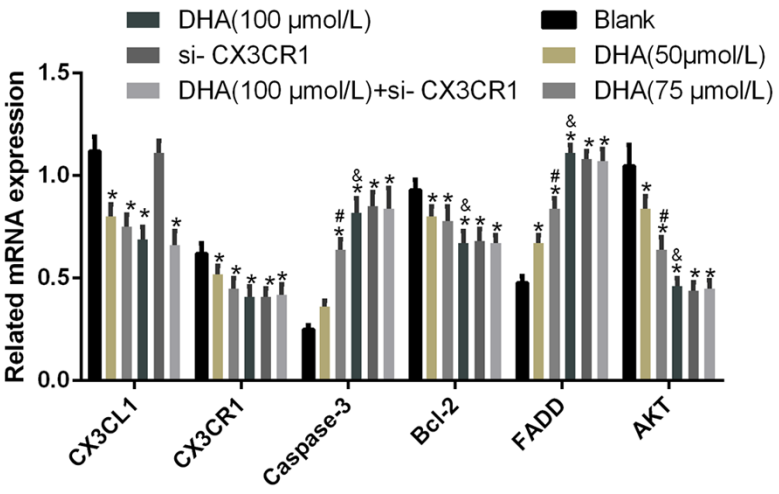

Figure 2. mRNA expression of CX3CL1, CX3CR1, caspase-3, Bcl-2, FADD, and AKT in each group by qRT-PCR. Note: *P<0.05, compared to the Blank group; #P<0.05, compared with the DHA (50 μmol/L) group; &P<0.05, compared with the DHA (75 μmol/L) group; n=3.

Statistical analysis

Statistical data were analyzed using the SPSS software (21.0, IBM, USA), version 21.0. Measurement data are described as mean ± sd and analyzed with the use of one-way ANOVA with post-hoc Bonferroni test. Each experiment was repeated at least 3 times. Significance was set at P<0.05.

Results

The microscopy shows successful transfection

Fluorescence microscopy revealed that cells in the Blank group had no fluorescence, whereas those in the si-CX3CR1 group were exposed to excitation light, and emitted diffusely distributed bright fluorescence (**Figure 1A**). If the recombinant plasmids were successfully transfected in the cells, and the expression rate of GFP reached over 92%, it suggested that the transfection efficiency was higher than 92% (**Figure 1B**).

DHA inhibits the mRNA expression of CX3CR1 and ligand CX3CR1, promotes the mRNA expression of apoptosis-related caspase-3 and FADD, and inhibits the mRNA expression of anti-apoptosis Bcl-2

The qRT-PCR indicated that when compared to the Blank group, the mRNA levels of CX3CL1, CX3CR1, Bcl-2, and AKT were lowered remarkably, but the mRNA levels of Caspase-3 and FADD rose substantially in the cells of the DHA (50 μmol/L) group, the DHA (75 μmol/L) group, the DHA (100 μmol/L) group, and the DHA (100 μmol/L) + si-CX3CR1 group (all P<0.05). Nevertheless, the mRNA levels of CX3CL1, CX3CR1, Bcl-2, Caspase-3, FADD and AKT differed insignificantly between the DHA (100 μmol/L) + si-CX3CR1 group and the DHA (100 μmol/L) group (all P>0.05). In the si-CX3CR1 group, substantive reductions in the mRNA expression of CX3CR1, Bcl-2 and AKT, but great improvements in mRNA expression of Caspase-3 and FADD were observed (all P<0.05). CX3CL1 mRNA expression varied insignificantly (P>0.05). Significant decreases in the mRNA expression of CX3CL1, CX3CR1, Bcl-2, and AKT, and increases in the Caspase-3 and FADD mRNA expression were present with the rise of DHA concentrations (**Figure 2**).

DHA suppresses the protein expression of CX3CR1 and ligand CX3CR1, improves the protein expression of apoptosis-related caspase-3 and FADD, and suppresses the protein expression of anti-apoptosis Bcl-2

Western blot electrophoresis demonstrated that as compared with the Blank group, the protein levels of CX3CL1, CX3CR1, Bcl-2, AKT, and p-AKT were lowered considerably, but those of caspase-3 and FADD rose greatly in the cells of the DHA (50 μmol/L) group, the DHA (75 μmol/L) group, the DHA (100 μmol/L) group, and the DHA (100 μmol/L) + si-CX3CR1 group (all P<0.05). Nevertheless, the protein levels of CX3CL1, CX3CR1, Bcl-2, caspase-3, FADD, AKT and p-AKT varied insignificantly between the DHA (100 μmol/L) + si-CX3CR1 group and the DHA (100 μmol/L) group (all P>0.05). In the si-CX3CR1 group, substantive reductions in the protein expression of CX3CR1, Bcl-2, AKT, and p-AKT, but great improvements in the protein expression of caspase-3 and FADD were seen

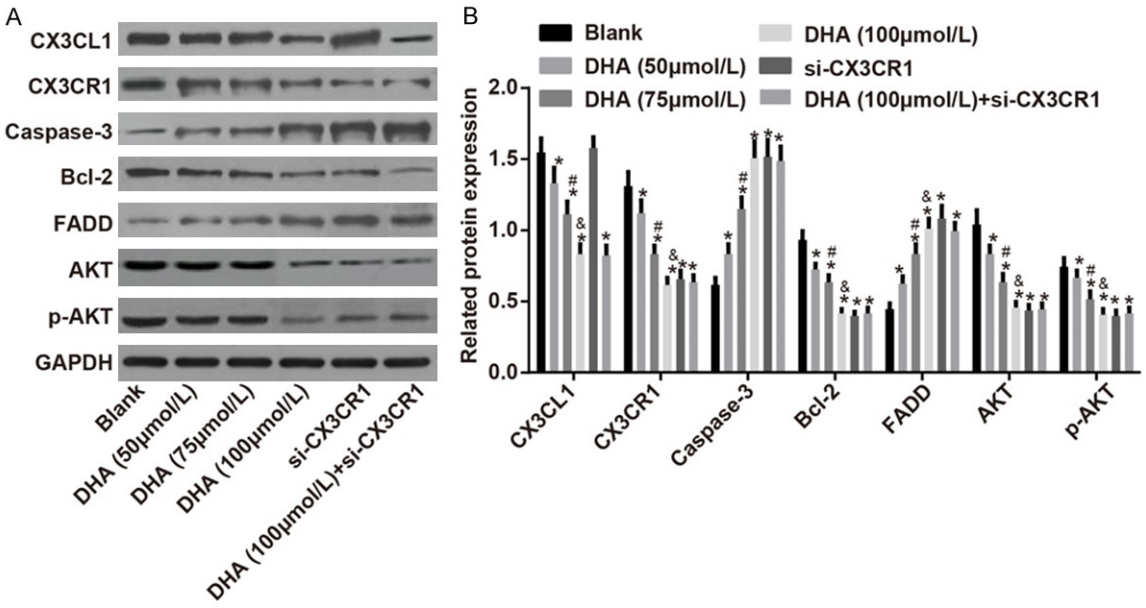

Figure 3. Western blot electrophoresis demonstrated the protein expression of CX3CL1, CX3CR1, caspase-3, Bcl-2, FADD, AKT, and p-AKT in all groups. Note: A: Western blot electrophoresis bands; B: Protein profiles of CX3CL1, CX3CR1, caspase-3, Bcl-2, FADD, AKT, and p-AKT in all groups. *P<0.05, compared with the Blank group; #P<0.05, compared with the DHA (50 μmol/L) group; &P<0.05, compared with the DHA (75 μmol/L) group; n=3.

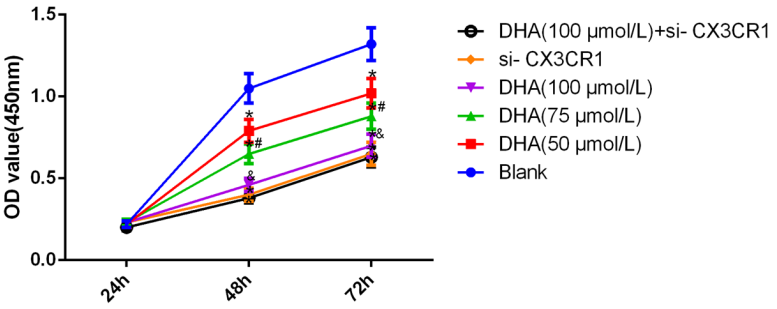

Figure 4. Statistical chart of cell proliferation at 24, 48, and 72 hours of all the groups in the CCK-8 assay. Note: *P<0.05, compared to the Blank group; #P<0.05, compared to the DHA (50 μmol/L) group; &P<0.05, compared to the DHA (75 μmol/L) group; n=3.

(all P<0.05); no substantive difference was shown in the protein expression of CX3CL1 (P>0.05). With the rise of DHA concentrations, considerable decreases in the protein expression of CX3CL1, CX3CR1 and Bcl-2, but increases in caspase-3 and FADD protein expression were noted in the cells (**Figure 3**).

Inhibition of U251 cell proliferation by DHA and CX3CR1 knockdown

The CCK-8 assay suggested that with the extension of culture time, the optical density (OD) values of the cells in the Blank group, the DHA (50 μmol/L) group, the DHA (75 μmol/L) group, the DHA (100 μmol/L) group, and the si-CX3CR1 group increased gradually (all P<0.05). At 48 and 72 hours, compared to the Blank group, the proliferation of cells declined considerably in the DHA (50 μmol/L) group, the DHA (75 μmol/L) group, the DHA (100 μmol/L) group, the si-CX3CR1 group, and the DHA (100 μmol/L) + si-CX3CR1 group (all P<0.05). No substantive disparity was noted in cell proliferation between the DHA (100 μmol/L) group and the DHA (100 μmol/L) + si-CX3CR1 group (all P>0.05). More potent cell proliferation was seen in the DHA (50 μmol/L) group than in the DHA (75 μmol/L) group, whereas the latter had more potent cell proliferation than the DHA (100 μmol/L) group (**Figure 4**).

Inhibition of U251 cell migration by DHA and CX3CR1 knockdown

Wound healing assay showed that with the extension of culture time, the migration of the

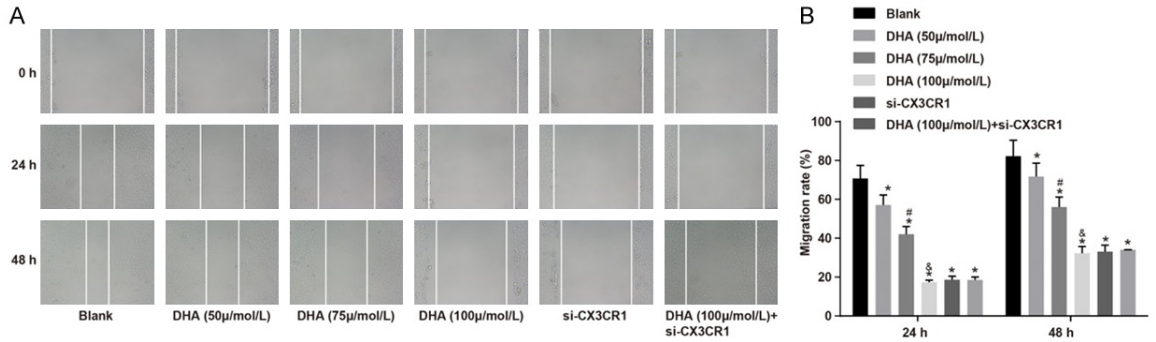

Figure 5. Statistical chart showing the migration distance and rates of cells in all the groups at 24 and 48 hours in the wound healing assay. Note: A: Micrograph of cell migration in the wound healing assay (40×); B: Statistical chart showing cell migration and wound healing. *P<0.05, compared with the Blank group; #P<0.05, compared to the DHA (50 μmol/L) group; &P<0.05, compared to the DHA (75 μmol/L) group; n=3.

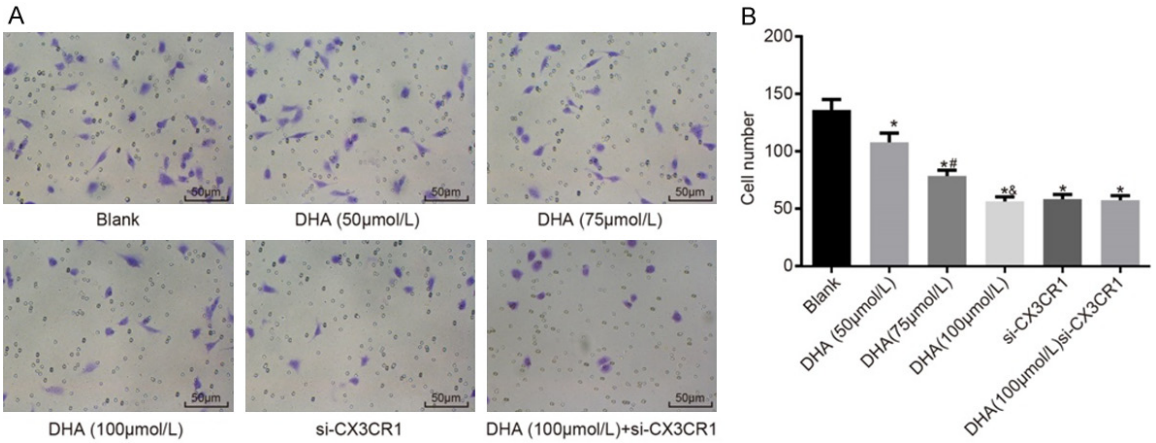

Figure 6. Micrographs of the invasive chambers and statistical chart of invasive cell number in the Transwell assay. Note: A: Micrograph of invasive chambers (200×); B: Statistical chart of transmembrane cell number. *P<0.05, compared with the Blank group; #P<0.05, compared to the DHA (50 μmol/L) group; &P<0.05, compared to the DHA (75 μmol/L) group; n=3.

cells in the Blank group, the DHA (50 μmol/L) group, the DHA (75 μmol/L) group, the DHA (100 μmol/L) group, and the si-CX3CR1 group improved gradually (all P<0.05). When compared to the Blank group, the migration of cells declined substantially in the DHA (50 μmol/L) group, the DHA (75 μmol/L) group, the DHA (100 μmol/L) group, the si-CX3CR1 group, and the DHA (100 μmol/L) + si-CX3CR1 group at 24 and 48 hours, respectively (all P<0.05). No significant changes in cell migration were noted in the DHA (100 μmol/L) group, and the DHA (100 μmol/L) + si-CX3CR1 group (all P>0.05). At 24 and 48 hours, cell migration was more viable in the DHA (50 μmol/L) group than in the DHA (75 μmol/L) group, whereas the latter had more viable cell migration than the DHA (100 μmol/L) group (**Figure 5**).

Inhibition of U251 cell invasion by DHA and CX3CR1 knockdown

The transwell invasion assay demonstrated that compared with the Blank group, the invasion of cells in the DHA (50 μmol/L) group, the DHA (75 μmol/L) group, the DHA (100 μmol/L) group, the si-CX3CR1 group, and the DHA (100 μmol/L) + si-CX3CR1 group declined remarkably (all P<0.05). At 48 and 72 hours, no significant changes in cell invasion were observed in the DHA (100 μmol/L) group and the DHA (100 μmol/L) + si-CX3CR1 group (all P>0.05). Cell invasion was more potent in the DHA (50 μmol/L) group than in the DHA (75 μmol/L) group, whereas the latter had more potent cell invasion than the DHA (100 μmol/L) group (**Figure 6**).

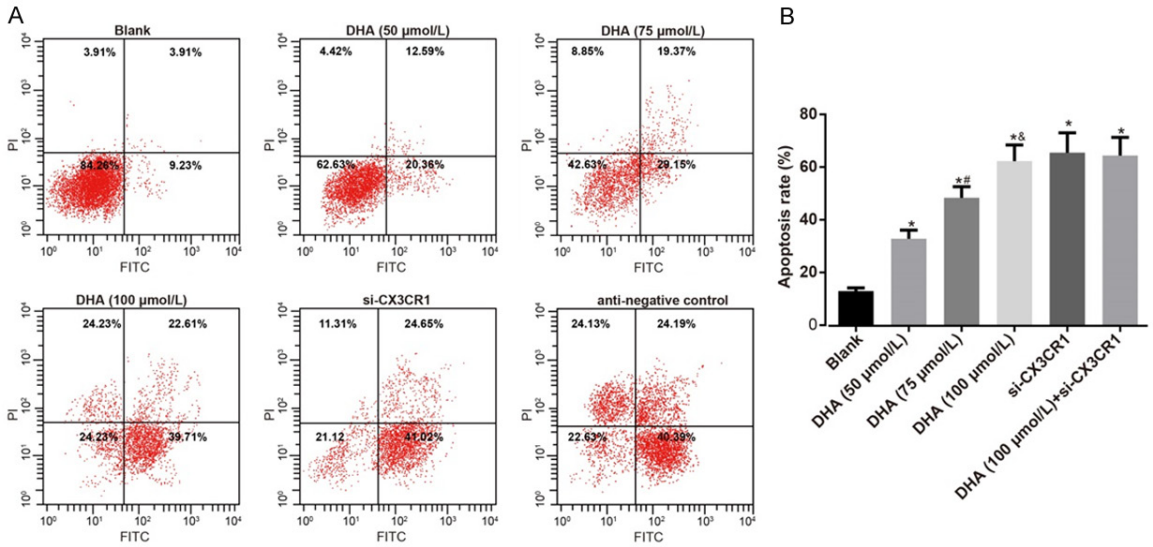

Figure 7. Histograms of apoptosis and statistical chart of the cell apoptosis rates of all the groups in the flow cytometry analysis. Note: A: Chart of apoptosis distribution; B: Statistical chart of apoptotic rates of cells. *P<0.05, compared to the Blank group; #P<0.05, compared to the DHA (50 μmol/L) group; &P<0.05, compared to the DHA (75 μmol/L) group; n=3.

Enhancement of U251 cell apoptosis by DHA and CX3CR1 knockdown

Flow cytometry analysis indicated that compared with the Blank group, the apoptosis of cells were improved strikingly in the DHA (50 μmol/L) group, the DHA (75 μmol/L) group, the DHA (100 μmol/L) group, the si-CX3CR1 group, and the DHA (100 μmol/L) + si-CX3CR1 group (all P<0.05). At 48 and 72 hours, insignificant variation in cell apoptosis was observed in the DHA (100 μmol/L) group and the DHA (100 μmol/L) + si-CX3CR1 group (all P>0.05). Cell apoptosis was more impotent in the DHA (50 μmol/L) group than in the DHA (75 μmol/L) group, whereas the latter had more impotent cell apoptosis than the DHA (100 μmol/L) group (**Figure 7**).

Discussion

Clinically, neuroma is frequently defined as the tumor in the nerve sheath tissue. Neuromas are mostly located in the axillary and limbs of patients, but may also appear in the neck, clavicle and other parts of the body. Currently, neuromas are primarily managed by surgical resection, radiotherapy and chemotherapy, as well as other adjuvant treatments. However, the therapeutic effect is not satisfactory. Recent studies suggest that DHA use is associated with promotion of apoptosis of tumor cells and enhancement of the sensitivity of tumor cells to radiation and chemotherapeutic drugs. However, the mechanism by which DHA affects tumor cells warrants further elucidation [9-11]. Previous literature indicates that DHA inhibits the PI3-K/Akt and ERK pathways controlling cell survival and triggers induction of the death receptor DR5 and activation of extrinsic and endogenous apoptotic signaling pathways [12]. DHA targets Janus kinase 2/signal transductor and transcriptional activator 3 signaling pathways to promote apoptosis of cancer cells [13]. DHA has also shown to inhibit proliferation of endothelial cells by suppressing the ERK signaling pathway [14-16]. Currently, multiple studies have been involved in the mechanisms of action of DHA. Nevertheless, additional studies are still needed for more profound exploration. This study was aimed to delve into the effect of DHA on cell apoptosis by regulating the CX3CR1 signaling pathway. We found that the pro-apoptotic effect of DHA on neuroma cells was concentration-dependent. The pro-apoptosis of DHA is increasingly effective with the increase of concentration.

CX3C chemokine receptor 1 (CX3CR1), also known as the fractalkine receptor or G-protein coupled receptor 13 (GPR13), is a human protein encoded by the CX3CR1 gene [16-18]. The

receptor binds to the chemokine CX3CL1 (also called neurotrophic factor or fractalkine). CX3CR1 signaling pathway plays a role in the migration of microglia in the central nervous system to their synaptic targets. Studies have shown that CX3CR1-knockout mice show more synapses on cortical neurons than wild-type mice [19]. Chemokines can alter migration of cancer cells and accelerate the progression of tumors, and their receptors can mediate the homing of cancer cells, and further enhance their invasion and migration [20-22]. CXCR4 and c-Kit can regulate cell proliferation, cytoskeletal function, and signal transduction in small cell lung cancer cells [23]. Fractalkine/CX3CR1 induces cell apoptotic resistance and proliferation by activating the AKT/NF-κB cascade in pancreatic cancer cells [24]. CX3CR1 regulates proliferation and apoptosis of chondrocytes in osteoarthrosis via Wnt/β-catenin signaling pathway [25].

The results of the current study demonstrated that DHA regulated the CX3CR1 signaling pathway and inhibited invasion and migration of neuroma cells and promoted their apoptosis. The findings of the qRT-PCR and Western blot demonstrated that DHA could inhibit the CX3CR1 signaling pathway and suppress the mRNA and protein expression of CX3CL1, CX3CR1, and Bcl-2, but elevated the mRNA and protein expression of FADD and caspase-3 in U251 cells. Furthermore, its effect was concentration-dependent. The CCK-8, wound healing, and transwell assays revealed that DHA could inhibit proliferation, migration and invasion of U251 cells and was also concentration-dependent. In the flow cytometry analysis, DHA could promote the apoptosis of U251 cells, and was also concentration-dependent. There were no significant disparities in expression, proliferation, migration and invasion of cell-associated factors, and apoptosis between the DHA (100 μmol/L) group and the si-CX3CR1 group, suggesting that DHA can really inhibit the CX3CR1 signaling pathway.

A study involving the relationship between DHA and treatment of glioma revealed that DHA could inhibit proliferation of glioma cells, and the mechanism is that DHA helps suppress the expression of vital protease MMP-2, and MMP-9 in the process of tumor invasion [26]. CX3CR1 is also a receptor of the irregular regulatory factor (Fkn), and both CX3CR1 and Fkn are expressed in many tissues and organs (nervous tissue, skin, and the kidneys). Another study investigating the relationship between FKN-CX3CR1 and the pathogenesis of atherosclerosis found that FKN-CX3CR1 has an inhibitory effect on MMP-2 expression in mononuclear cells [27]. Therefore, we hold that the mechanism by which DHA regulates the CX3CR1 signaling pathway, inhibits the invasion and migration of neuroma cells, and promotes the apoptosis of neuroma cells may correlate with the effect of CX3CR1 signaling pathway on the MMP-2 expression.

These findings may bring some insights into the management of neuroma with DHA in the future. However, relevant toxicity tests, animal experiments, and *in vivo* trials are still required for further confirmation. CX3CR1 can activate numerous downstream signaling pathways (PI3K and ERK5). In the present study, we only conducted some research on CX3CR1, and found that DHA could inhibit the activity of AKT. Nevertheless, we have not conducted specific studies on the DHA-activated downstream pathways. Follow-up studies are still needed to reveal how DHA mediates the downstream pathways by regulating the CX3CR1 expression, and specific mechanisms warrant further exploration.

Disclosure of conflict of interest

None.

Address correspondence to: Xia Liu, Department of Pathology, Xuzhou Central Hospital, The Affiliated Xuzhou Hospital of Medical College of Southeast University, Xuzhou Clinical School of Xuzhou Medical College, No. 199 Jiefang South Road, Xuzhou City 221009, Jiangsu Province, P.R. China. Tel: +86-0516-83956524; E-mail: xialiu179@163.com

References

[1] Wu G, Diaz AK, Paugh BS, Rankin SL, Ju B, Li Y, Zhu X, Qu C, Chen X, Zhang J, Easton J, Edmonson M, Ma X, Lu C, Nagahawatte P, Hedlund E, Rusch M, Pounds S, Lin T, Onar-Thomas A, Huether R, Kriwacki R, Parker M, Gupta P, Becksfort J, Wei L, Mulder HL, Boggs K, Vadodaria B, Yergeau D, Russell JC, Ochoa K, Fulton RS, Fulton LL, Jones C, Boop FA, Broniscer A, Wetmore C, Gajjar A, Ding L, Mardis ER, Wilson RK, Taylor MR, Downing JR, Ellison DW, Zhang J and Baker SJ. The genomic landscape of dif-

fuse intrinsic pontine glioma and pediatric non-brainstem high-grade glioma. Nat Genet 2014; 46: 444-450.
[2] Chen J, Chen X, Wang F, Gao H and Hu W. Dihydroartemisinin suppresses glioma proliferation and invasion via inhibition of the ADAM17 pathway. Neurol Sci 2015; 36: 435-440.
[3] Mao H, Gu H, Qu X, Sun J, Song B, Gao W, Liu J and Shao Q. Involvement of the mitochondrial pathway and Bim/Bcl-2 balance in dihydroartemisinin-induced apoptosis in human breast cancer in vitro. Int J Mol Med 2013; 31: 213-218.
[4] Zhang ZS, Wang J, Shen YB, Guo CC, Sai KE, Chen FR, Mei X, Han FU and Chen ZP. Dihydroartemisinin increases temozolomide efficacy in glioma cells by inducing autophagy. Oncol Lett 2015; 10: 379-383.
[5] Qu C, Ma J, Liu X, Xue Y, Zheng J, Liu L, Liu J, Li Z, Zhang L and Liu Y. Dihydroartemisinin exerts anti-tumor activity by inducing mitochondrion and endoplasmic reticulum apoptosis and autophagic cell death in human glioblastoma cells. Front Cell Neurosci 2017; 11: 310.
[6] Freria CM, Hall JC, Wei P, Guan Z, McTigue DM and Popovich PG. Deletion of the fractalkine receptor, CX3CR1, improves endogenous repair, axon sprouting, and synaptogenesis after spinal cord injury in mice. J Neurosci 2017; 37: 3568-3587.
[7] Poniatowski LA, Wojdasiewicz P, Krawczyk M, Szukiewicz D, Gasik R, Kubaszewski L and Kurkowska-Jastrzebska I. Analysis of the role of CX3CL1 (fractalkine) and its receptor CX3CR1 in traumatic brain and spinal cord injury: insight into recent advances in actions of neurochemokine agents. Mol Neurobiol 2017; 54: 2167-2188.
[8] He F, Zhang RY, Wang J, Deng F, Fan MT, Li Y, Guo YL and Shi Q. Effects of expression silencing of chemokine receptor CX3CR1 on human hepatocellular carcinoma Huh7 cells and its machanism. Tumor 2015; 35: 46-54.
[9] Xu G, Zou WQ, Du SJ, Wu MJ, Xiang TX and Luo ZG. Mechanism of dihydroartemisinin-induced apoptosis in prostate cancer PC3 cells: an iTRAQ-based proteomic analysis. Life Sci 2016; 157: 1-11.
[10] Zhang T, Hu Y, Wang T and Cai P. Dihydroartemisinin inhibits the viability of cervical cancer cells by upregulating caveolin 1 and mitochondrial carrier homolog 2: Involvement of p53 activation and NAD(P)H: quinone oxidoreductase 1 downregulation. Int J Mol Med 2017; 40: 21-30.
[11] He Q, Shi J, Shen XL, An J, Sun H, Wang L, Hu YJ, Sun Q, Fu LC, Sheikh MS and Huang Y. Dihydroartemisinin upregulates death receptor 5 expression and cooperates with TRAIL to induce apoptosis in human prostate cancer cells. Cancer Biol Ther 2010; 9: 819-824.
[12] Wang D, Zhong B, Li Y and Liu X. Dihydroartemisinin increases apoptosis of colon cancer cells through targeting Janus kinase 2/signal transducer and activator of transcription 3 signaling. Oncol Lett 2018; 15: 1949-1954.
[13] Dong F, Tian H, Yan S, Li L, Dong X, Wang F, Li J, Li C, Cao Z, Liu X and Liu J. Dihydroartemisinin inhibits endothelial cell proliferation through the suppression of the ERK signaling pathway. Int J Mol Med 2015; 35: 1381-1387.
[14] Wang Y, Cao J, Fan Y, Xie Y, Xu Z, Yin Z, Gao L and Wang C. Artemisinin inhibits monocyte adhesion to HUVECs through the NF-kappaB and MAPK pathways in vitro. Int J Mol Med 2016; 37: 1567-1575.
[15] Hwang YP, Yun HJ, Kim HG, Han EH, Lee GW and Jeong HG. Suppression of PMA-induced tumor cell invasion by dihydroartemisinin via inhibition of PKCalpha/Raf/MAPKs and NF-kappaB/AP-1-dependent mechanisms. Biochem Pharmacol 2010; 79: 1714-1726.
[16] Combadiere C, Ahuja SK and Murphy PM. Cloning, chromosomal localization, and RNA expression of a human beta chemokine receptor-like gene. DNA Cell Biol 1995; 14: 673-680.
[17] Combadiere C, Salzwedel K, Smith ED, Tiffany HL, Berger EA and Murphy PM. Identification of CX3CR1. A chemotactic receptor for the human CX3C chemokine fractalkine and a fusion coreceptor for HIV-1. J Biol Chem 1998; 273: 23799-23804.
[18] Ensan S, Li A, Besla R, Degousee N, Cosme J, Roufaiel M, Shikatani EA, El-Maklizi M, Williams JW, Robins L, Li C, Lewis B, Yun TJ, Lee JS, Wieghofer P, Khattar R, Farrokhi K, Byrne J, Ouzounian M, Zavitz CC, Levy GA, Bauer CM, Libby P, Husain M, Swirski FK, Cheong C, Prinz M, Hilgendorf I, Randolph GJ, Epelman S, Gramolini AO, Cybulsky MI, Rubin BB and Robbins CS. Self-renewing resident arterial macrophages arise from embryonic CX3CR1(+) precursors and circulating monocytes immediately after birth. Nat Immunol 2016; 17: 159-168.
[19] Paolicelli RC, Bolasco G, Pagani F, Maggi L, Scianni M, Panzanelli P, Giustetto M, Ferreira TA, Guiducci E, Dumas L, Ragozzino D and Gross CT. Synaptic pruning by microglia is necessary for normal brain development. Science 2011; 333: 1456-1458.
[20] Amit M, Na'ara S and Gil Z. Mechanisms of cancer dissemination along nerves. Nat Rev Cancer 2016; 16: 399-408.
[21] Marchesi F, Piemonti L, Mantovani A and Allavena P. Molecular mechanisms of perineural invasion, a forgotten pathway of dissemination and metastasis. Cytokine Growth Factor Rev 2010; 21: 77-82.

[22] Shen F, Zhang Y, Jernigan DL, Feng X, Yan J, Garcia FU, Meucci O, Salvino JM and Fatatis A. Novel small-molecule CX3CR1 antagonist impairs metastatic seeding and colonization of breast cancer cells. Mol Cancer Res 2016; 14: 518-527.

[23] Kijima T, Maulik G, Ma PC, Tibaldi EV, Turner RE, Rollins B, Sattler M, Johnson BE and Salgia R. Regulation of cellular proliferation, cytoskeletal function, and signal transduction through CXCR4 and c-Kit in small cell lung cancer cells. Cancer Res 2002; 62: 6304-6311.

[24] Wang H, Cai J, Du S, Guo Z, Xin B, Wang J, Wei W and Shen X. Fractalkine/CX3CR1 induces apoptosis resistance and proliferation through the activation of the AKT/NF-kappaB cascade in pancreatic cancer cells. Cell Biochem Funct 2017; 35: 315-326.

[25] Sun Y, Wang F, Sun X, Wang X, Zhang L and Li Y. CX3CR1 regulates osteoarthrosis chondrocyte proliferation and apoptosis via Wnt/beta-catenin signaling. Biomed Pharmacother 2017; 96: 1317-1323.

[26] Cao L, Duanmu W, Yin Y, Zhou Z, Ge H, Chen T, Tan L, Yu A, Hu R, Fei L and Feng H. Dihydroartemisinin exhibits anti-glioma stem cell activity through inhibiting p-AKT and activating caspase-3. Pharmazie 2014; 69: 752-758.

[27] Zou W, Liu ZY, Sun XW, Teng W and Jia N. Study on the relationship among MMP-2, atherosclerosis and cerebral infarction. Chinese Archives of Traditional Chinese Medicine 2012.